UNIVERSITY OF OKLAHOMA

GRADUATE COLLEGE

# UPPER TROPOSPHERE LOWER STRATOSPHERE COMPOSITION CHANGE IN TROPICAL CYCLONES: ASSESSMENTS FROM 17 YEARS OF SATELLITE OBSERVATIONS

A THESIS

SUBMITTED TO THE GRADUATE FACULTY

in partial fulfillment of the requirements for the

Degree of

MASTER OF SCIENCE

By

Hannah Fagan
Norman, Oklahoma
2025

UPPER TROPOSPHERE LOWER STRATOSPHERE COMPOSITION CHANGE IN TROPICAL CYCLONES: ASSESSMENTS FROM 17 YEARS OF SATELLITE OBSERVATIONS

A THESIS APPROVED FOR THE
SCHOOL OF METEOROLOGY

BY THE COMMITTEE CONSISTING OF

Dr. Cameron Homeyer (Chair)

Dr. Steven Cavallo

Dr. James Ruppert

## Acknowledgments

I would first like to acknowledge that none of this work would have been possible if not for my advisor Dr. Cameron Homeyer, who supported me and provided extensive feedback as I pursued this research. I have him to thank for exposing me to the joys of the UTLS world and the horrors of debugging IDL code (although the outcome was indisputably worth those frustrating hours). I would also like to thank fellow CCC research group members Andrea Gordon and Cole Shepherd as well as CCC alumnus Dr. Emily Tinney for their camaraderie throughout my time at OU. Additionally, thank you to my committee members Dr. Steven Cavallo and Dr. James Ruppert for enduring the first draft of this thesis and supporting my work; without assistance, this document would likely be unreadable!

I want to extend my gratitude to all of my office mates in NWC 5700, both past and present, who made me laugh and kept me going when things were difficult. I would also like to acknowledge the contributions of my friends at OU SoM, including Nick Amundsen and his fiance Emma Wood, Ryan Martz, and Emily West, as well as my friends from Florida State such as Jonathan Marcus, Riley Winch, Patrice Minogue, Thomas Silas, and Nick Amundsen again, who deserves particular credit for putting up with me since we were both undergraduate meteorology students and synoptic meteorology lab partners at FSU. Although they are presently illiterate, I also must thank my cats Biscuit and Nutmeg for providing me with the stress relief I needed while I wrote this thesis, as well as my childhood cats Snowball, Scout, and Murph for always welcoming me home whenever I needed a break from graduate student life. Finally, I would like to thank my family for the support throughout this process, especially my mother, who listened to my numerous phone call rants throughout this process. I truly don't know what I would do without such an amazing support network. Thank you all!

# Table of Contents

# List of Tables

## List of Figures

## Abstract

Tropical cyclones (TCs) are known for a variety of impacts, including threats to life and property, although their effect on the chemical composition of the upper troposphere and lower stratosphere (UTLS) remains understudied. The transport of air between the troposphere and stratosphere, known as stratosphere-troposphere exchange (STE), involves greenhouse gases such as ozone and water vapor whose impact on Earth's radiation budget and climate is most sensitive to changes in UTLS composition. Therefore, we examine observations of STE in TCs and relate these changes to TC and environmental characteristics. We utilize 17 years of trace gas profiles from the Microwave Limb Sounder (MLS) aboard the Aura satellite in conjunction with TC track information and environmental data to relate UTLS ozone and water vapor changes to TC intensity, distance from TC center, and environmental wind shear. We find that accounting for varying tropopause heights and basin-specific background composition is important to accurate assessment of UTLS composition changes within a TC. We also find that TCs are associated with increased water vapor throughout most of the UTLS and dehydration at tropopause level, while ozone is reduced greatly in the upper troposphere. All diagnosed UTLS composition changes demonstrate significant sensitivity to distance from TC center and TC intensity. Additionally, we find that TC-induced UTLS $H_2O$ changes are highly dependent on shear magnitude, where weaker shear is associated with more pronounced tropospheric hydration and tropopause dehydration.

# Chapter 1

# Introduction

Stratosphere-troposphere exchange (STE) is the critical process by which chemically distinct stratospheric air is irreversibly transported to the troposphere or vice versa (Holton et al. 1995). To diagnose STE, ozone ($O_3$) can be used as a stratospheric tracer (Rodgers et al. 1990); the concentration of $O_3$ is high in the stratosphere and uniformly low in the troposphere. Analogously, water vapor ($H_2O$) commonly serves as a tracer of tropospheric air. Both $H_2O$ and $O_3$ are critical greenhouse gases; $H_2O$ is a major contributor to global radiative forcing, including in the stratosphere, where decreases in concentration have been linked to slower global surface temperature increases (Kiehl and Trenberth 1997; Solomon et al. 2010). Additionally, the radiative sensitivity to $H_2O$ change is largest within the lower stratosphere (Banerjee et al. 2019), and therefore small composition changes can have large climate impacts. Similarly, the vertical distribution of $O_3$ plays a critical radiative role, as reductions in upper troposphere and lower stratosphere (UTLS) $O_3$ concentration are associated with surface cooling (Lacis et al. 1990). Thus, the resulting changes in UTLS chemical composition driven by STE have profound implications for Earth's climate system (Holton et al. 1995). Despite the known importance of UTLS composition, our understanding of STE processes and mixing remain limited (Riese et al. 2012). Therefore, developing a better understanding of STE pathways is critical to improvements in modeling Earth's radiative budget.

Past work has identified numerous processes that affect the chemical composition of the UTLS. It has been observed that tropospheric air enters the stratosphere in the tropics, travels poleward within the stratosphere, and sinks back into the troposphere in the extratropics; this slow transport is known as the Brewer-Dobson circulation (Brewer 1949; Dobson 1956) and is driven by extratropical pumping induced by dissipating planetary-scale and gravity waves in the stratosphere (Butchart 2014). Of these, breaking Rossby waves dominate (Holton et al. 1995). In addition to their dynamical impact on stratospheric circulation, Rossby wave breaking events can also impact the chemical composition of the UTLS when they occur near the tropopause, especially along isentropic surfaces near the subtropical jet (McIntyre and Palmer 1983; Liu and Barnes 2018). Isentropic exchange also occurs within tropopause folds, where stratospheric and tropospheric air overturn due to ageostrophic circulations in upper tropospheric jets and within frontal zones (Shapiro 1980; Keyser and Shapiro 1986). Although tropopause folding represents a majority of STE in the midlatitudes, more rapid processes such as overshooting deep convection have been observed (Jellis et al. 2023; Homeyer and Bowman 2021); over tropical landmasses, this overshooting convection has been shown to contribute significantly to STE and UTLS composition (Pommereau 2010). These processes demonstrate the necessity of considering numerous dynamical phenomena when analyzing UTLS composition and its evolution.

Tropical cyclones (TCs) are another type of weather phenomena that facilitates STE. TCs have a lifespan of days to weeks and are associated with modifications to large-scale upper tropospheric flow (Merrill 1988), increases in upper tropospheric $H_2O$ (Ray and Rosenlof 2007), and decreases in upper tropospheric $O_3$ (Zhan and Wang 2012). Although TCs comprise a small fraction of deep tropical convection, they represent a disproportionate amount of tropopause-overshooting convection in this region ($\approx$30%; Romps and Kuang 2009) and can induce up to 30% of tropical troposphere-to-stratosphere transport (Zhan and Wang 2012); therefore, given their relatively long lifespan in comparison to other phenomena, evaluating the effects of STE within TCs is critical. Furthermore, TC intensity is projected to increase in a warming climate (Emanuel 1987), and overshooting convection frequency is expected to exponentially increase with increasing SSTs (Griffin 2017). Therefore, it is essential to investigate the relationship between storm strength and STE within TCs, particularly given the potential feedback loop between TCs and the global climate system.

Previous studies have outlined some STE mechanisms within TCs. Danielsen (1993) found evidence of a lifted tropopause within TCs which intersects UTLS isentropes. Resulting isentropic mixing facilitates the transport of tropospheric air into the lower stratosphere. Within the troposphere, downward transport associated with TC outflow has led to the intrusion of stratospheric air near the outflow edge (Leclair De Bellevue et al. 2006), particularly in strong cyclones (Baray et al. 1999). Additionally, modeling work has shown the importance of overshooting tops within TCs. Overshooting tops have been associated with robust two-way exchange, particularly within the outer rainbands, despite their small scale (Allison et al. 2018; Preston et al. 2019). Notably, Leclair De Bellevue et al. (2007) demonstrate a potential relationship between STE and vertical wind shear; given that the deepest convection occurs downshear of the core of TCs (DeHart et al. 2014), a further investigation of the relationship between shear and STE is warranted. Finally, within the TC eye, deep subsidence of stratospheric air into the troposphere has been observed and evidenced by increased upper tropospheric $O_3$ (Rodgers et al. 1990), although work by Joiner et al. (2006) showed negligible increases in $O_3$ within the eye of a TC when adjusted for cloud pressure. Decreased tropospheric and total column $O_3$ has also been associated with TCs (Newell et al. 1996; Zou and Wu 2005), indicating the dominance of upward transport of $O_3$-poor lower tropospheric air.

Aura Microwave Limb Sounder (MLS) satellite observations have been utilized to evaluate STE-induced UTLS composition change in TCs. When utilizing observations from the North Indian Ocean basin from a limited time period, Ratnam et al. (2016) found stratospheric $H_2O$ enhancement and increased tropospheric $O_3$ near TC center. Using MLS observations from 3 storms, Jiang et al. (2020) found that a $H_2O$ was reduced at tropopause level and increased in the stratosphere near TCs. Leveraging 2 years of MLS data, Ray and Rosenlof (2007) also found evidence of strong TC-induced hydration within the upper troposphere; the strength of the hydration was correlated with storm intensity, indicating a potential link between TC intensity and STE. Collectively, these studies reveal some observed composition changes resulting from STE within TCs, although they have used relatively limited sample sizes. Additionally, previous work has focused on a single ocean basin over a limited time period; therefore, a more complete analysis of STE within TCs is warranted.

Given the limitations of previous efforts to improve understanding of STE within TCs, we aim to address these gaps by leveraging a long, global record of satellite observations from the Aura MLS. Specifically, we examine the influence of TCs on UTLS $O_3$ and $H_2O$ composition over a 17-year period, from 2005 through 2021, representing the longest analyzed observational record of TC effects on the UTLS. This increased temporal coverage and sample size allow for detailed exploration of the relationship between UTLS composition impacts from TCs and storm characteristics, which we investigate in multiple coordinate systems to evaluate the validity of previously identified processes on a global scale. In particular, we investigate how storm intensity, radial distance from the TC center, and environmental deep-layer wind shear relate to changes in UTLS $O_3$ and $H_2O$; quantifying these impacts, particularly in terms of vertical distance from the tropopause, is critical to improving understanding of how TCs impact Earth's radiation budget and climate.

# Chapter 2

# Data & Methods

## 2.1 Aura MLS

The Aura satellite follows a sun-synchronous orbital track and MLS has produced nearly continuous profiles of atmospheric composition since its launch in 2004. For analysis, version 5 MLS profiles from 2005 through 2021 are used; data after 2021 are not included to avoid biases resulting from global stratospheric hydration following the 2022 Hunga Tonga-Hunga Ha'apai volcanic eruption Millán et al. (2022). MLS retrieves profiles every 160 km along orbit, with the spatial resolution, accuracy, precision, and retrieval ranges of $O_3$ and $H_2O$ retrievals recorded in Table 1 Livesey et al. (2022). Notably, the dataset has a relatively coarse spatial resolution; therefore, fine-scale details of TC-associated transport cannot be resolved using these satellite observations. However, the spatial resolution of observations is comparable to the scale of TCs and can be utilized to analyze overall UTLS composition changes in TCs with confidence (owing to robust statistics possible from large sample sizes).

## 2.2 IBTrACS

The International Best Track Archive for Climate Stewardship (IBTrACS; Knapp et al. 2010) is a comprehensive dataset that synthesizes TC track data from a variety of international reporting agencies. IBTrACS data contains information about the type of system (whether it is tropical, subtropical, or extratropical), as well as an intensity classification (disturbance, tropical wave, tropical depression, tropical storm, or hurricane). For this project, only tropical storms (sustained 10-m winds of 35–63 kts) and hurricanes (sustained

10-m winds of $\geq$64 kts) are considered due to diminishing UTLS impacts at low storm intensities (see Section 3.1). IBTrACS also includes TC location at 3-hour increments at a minimum, as well as data on TC strength and ocean basin of origin. In this analysis, TC profiles from the North Atlantic (NA), South Indian (SI), East Pacific (EP), West Pacific (WP), and South Pacific (SP) basins are utilized. These basins represent nearly all globally observed TCs within the 17-year analysis period, as illustrated in Fig. 2.1.

Using location data from both IBTrACS and MLS profiles, TC characteristics and UTLS composition data are matched, providing an abundant number of samples (summarized in Table 2.2). MLS profiles taken within 1.5 hours and 1000 km of a TC location are flagged as TC profiles, while non-TC profiles are between 1000 and 1500 km removed from the center of a TC (though sampled at the same times). These non-TC profiles provide a reference for the local background environment beyond the main circulation of the TC but are still representative of an environment in which a TC would form, limiting the effects of UTLS seasonal variability.

## 2.3 MERRA-2 Reanalysis

For environmental conditions, we use 3-hourly assimilations of the global atmosphere from the NASA Modern-Era Retrospective analysis for Research and Applications, Version 2 (MERRA-2). MERRA-2 spans 1979 to the present and has a horizontal resolution of 0.625$\times$0.5 degrees longitude-latitude with 72 vertical levels (corresponding to $\approx$1100-m grid spacing within the UTLS; Gelaro et al. 2017). MERRA-2 is suitable for this study because its representation of the tropopause and tropospheric winds are comparatively accurate to alternative reanalyses (Xian and Homeyer 2019; Wu et al. 2024), especially relative to the coarse resolution of the MLS profiles. The deep-layer (850–200 hPa) wind shear vector at 3-hourly intervals for each TC is computed following a common approach in TC studies (e.g., see Kaplan and DeMaria 2003; Chen et al. 2006; Hence and Houze 2011): the average value of all MERRA-2 grid points within an annular ring 200–800 km from TC center, aiming to mitigate influence from the primary circulation of the TC. For tropopause analysis, we apply the World Meteorological Organization (1957) lapse rate tropopause (LRT) definition to MERRA-2 analyses, which has been shown to identify the tropopause height more accurately within than the cold point tropopause definition when considering the tropics (Pan et al. 2018). This reanalysis data is matched with Aura MLS profiles via linear interpolation in space and time.

## 2.4 Tropopause-Relative Analysis

Because the troposphere and stratosphere are chemically distinct, it is important to evaluate changes in UTLS composition based on whether they occur above or below the tropopause. Thus, in order to accurately assess STE within TCs, MLS profiles are converted into tropopause-relative logarithmic pressure coordinates for both $O_3$ and $H_2O$ observations, minimizing the effect of variable tropopause heights on the resulting analysis of multiple profiles (see Fig. 2.2). First, tropopause pressure at the MLS profile locations is sourced from MERRA-2 reanalysis data. Next, 12 tropopause-relative bins are created for each profile at a resolution of 0.075 decades of pressure (equivalent to approximately 1 km of vertical distance in the UTLS, as done in Tinney and Homeyer (2021)). Trace gas concentrations are then averaged within tropopause-relative logarithmic pressure bins for comparison of MLS profile samples. Finally, tropopause-relative profiles are transformed back into pressure space for some analyses using the average tropopause pressure for all samples. This allows for reliable comparison of UTLS composition between profiles by avoiding contaminating stratospheric samples with tropospheric observations (and vice versa). This study is the first to employ this technique for the evaluation of UTLS composition change within TCs. Figure 2.3 shows the resulting bulk impacts on assessed UTLS composition change when using pressure coordinates and tropopause-relative coordinates. For $O_3$, these changes are most apparent for tropical storms, which seemingly result in increased UTLS

$O_3$ in standard pressure coordinates (Fig. 2.3a); however, when adjusting to a tropopause-relative framework, tropical storms clearly result in decreased UTLS $O_3$ (Fig 2.3c). This result removes the effects of mixing tropospheric and stratospheric air and is consistent with past work (e.g. Zou and Wu 2005). UTLS $H_2O$ patterns are similarly altered when converted to a tropopause-relative framework; for major hurricanes, $H_2O$ changes are positive throughout the UTLS in standard pressure coordinates (Fig. 2.3b), while in tropopause-relative coordinates there is a decrease in $H_2O$ near the tropopause (Fig. 2.3d). These UTLS composition changes are only visible in a tropopause-relative framework.

## 2.5 Basin Relative Analysis

There is great spatial variability in background concentrations of $O_3$ and $H_2O$ within the UTLS (see Figure 2.4), even within the tropics. Therefore, composition changes are best assessed relative to typical concentrations in the local TC environment. To accomplish this, background profiles are calculated and averaged in tropopause-relative coordinates for reference using only non-TC profiles taken over each basin. As summarized previously (see Section 2.2), these background calculations are restricted to samples from TC times to limit the impacts of seasonal variation. Figure 2.4 demonstrates the large observed variability in UTLS background composition between basins from MLS measurements, especially near and below the tropopause. For instance, $H_2O$ concentrations around the tropopause are on average around 3 ppmv for the SP and SI ocean basins; in contrast, the NA tropopause has a background concentration of $\approx$10 ppmv, more than triple some other basins, due to variability from meteorological and anthropogenic factors. Similar differences are found in the upper troposphere for $O_3$. Therefore, it is important to consider which basin a TC forms in to accurately evaluate STE and UTLS composition change. After identifying the ocean basin, the basin-averaged background composition is subtracted from each tropopause-relative TC profile and resulting differences are commensurately averaged to assess composition change. All subsequent analysis is performed using basin-relative considerations.

In Figure 2.5, we demonstrate the necessity of this method by analyzing samples of hurricane-intensity TCs. When considering profiles from the NA basin (relatively high background $O_3$ and $H_2O$ in the UTLS, as demonstrated in Fig. 2.4) and the SI basin (relatively low background $O_3$ and $H_2O$ in the UTLS), we find significant absolute concentration differences between basin and TC profiles. The $O_3$ concentration within NA TCs is significantly higher than the concentration within SI TCs throughout some parts of the upper troposphere (minima ≈50 ppbv versus ≈30 ppbv). UTLS $H_2O$ shows similar variations; near the tropopause, the average $H_2O$ concentration is ≈3 ppmv for SI TCs, but ≈10 ppmv for NA TCs (as previously mentioned). Changes relative to average basin-specific background profiles (Figs. 2.5c & 2.5d), however, demonstrate that assessed UTLS composition change becomes more comparable between basins when accounting for their respective backgrounds. There are some complex differences in the profiles of UTLS $H_2O$ changes from TCs, but the vertical structure is similar overall, such as hydration and reduced $O_3$ in the upper troposphere, a slightly drier tropopause region, and weak stratospheric hydration that is not as readily evident in the absolute concentration plots. Therefore, basin-relative analysis is essential for aggregating TC profiles and assessing UTLS composition change across ocean basins.

## 2.6 Limb Geometry

An important consideration when leveraging Aura MLS data for studying TCs is the geometry of the limb measurement. Namely, the width of the limb path is approximately 15 km for all MLS observables, but the length of the limb path (along the line of sight) varies by MLS observable and altitude. For UTLS observations, $H_2O$ limb lengths are 185–210 km, while $O_3$ limb lengths are much coarser at 300–450 km (see Table 2.1). Given such limb geometry, the orientation of the limb measurement relative to a TC determines its utility for assessing TC impacts on UTLS composition as a function of distance from TC center (radius). Figure 2.6 illustrates this relationship. Namely, Figs. 2.6a & 2.6b show the possible extremes of limb path orientation as that perpendicular to TC center (orientation = 0°) and parallel to TC center (orientation = 90°), respectively. Figs. 2.6c & 2.6d subsequently reveal the resulting radii from TC center limb lengths of 200 km and 400 km, respectively, would span at varying limb orientations and distances from TC center. Near TC center (within one-quarter the limb length), the radii span of a given measurement is generally insensitive to limb orientation as it is roughly collocated with TC center and equivalent to half the limb length. At distances from TC center greater than one-quarter the limb length, a large sensitivity in the radii spanned by a measurement arises due to limb orientation, with orientations $\leq 30°$ resulting in radii spans at or below those near TC center. For these reasons, we determine the limb orientation relative to TC center for all MLS profiles to facilitate analyses partitioned by distance from TC center. Specifically, for further analysis we retain all observations regardless of limb orientation at distances from TC center within one-quarter the limb length and restrict analyses at greater distances to profiles with limb orientations $\leq 30°$ only.

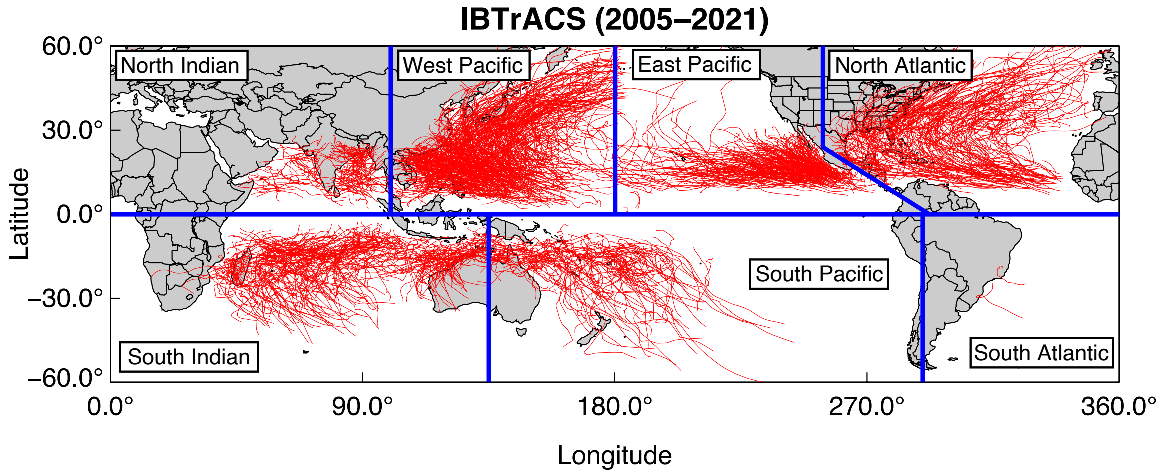


Figure 2.1: All IBTrACS TC tracks (red lines) within the analysis period (2005–2021). Longitude-latitude bounds of IBTrACS basins are indicated by thick blue lines.

Table 2.1: UTLS properties of ozone ($O_3$) and water vapor ($H_2O$) MLS observations.

| Gas | $\Delta x$ (km) | $\Delta z$ (km) | Precision | Accuracy | Retrieval Range |
|---|---|---|---|---|---|
| $O_3$ | 300–450 | 2.5–3.5 | 20–40 ppbv | +7–10% | 251–0.03 hPa |
| $H_2O$ | 185–210 | 1.4–3.1 | 5–40% | 8–25% | 316–0.002 hPa |

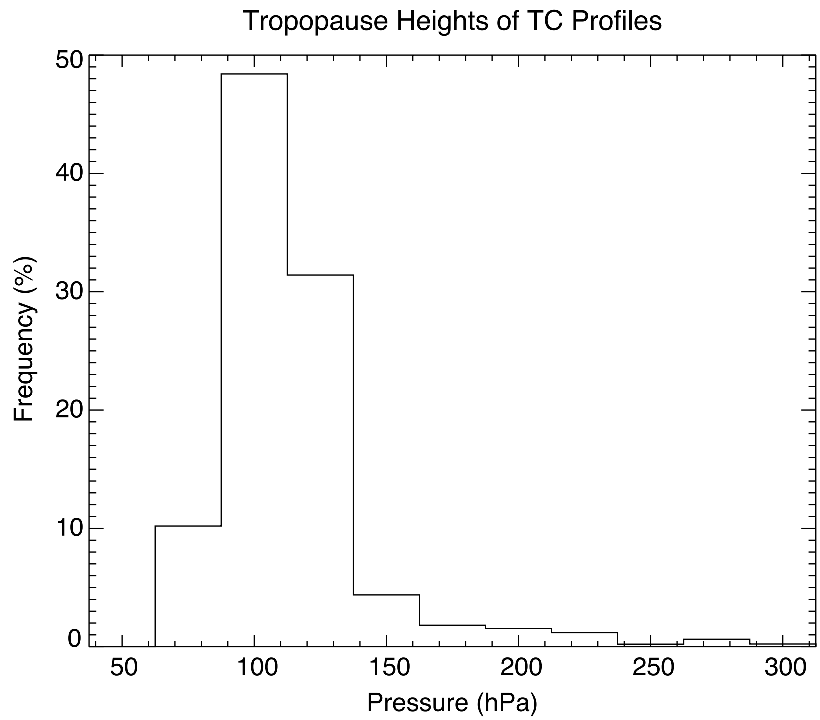


Figure 2.2: A histogram of tropopause heights of all utilized TC profiles.

Table 2.2: Number of TC and Background Profiles by Basin

| | WP | EP | SP | NA | SI | Total |
|---|---|---|---|---|---|---|
| Background (non-TC) profiles | 36,818 | 20,579 | 10,117 | 26,544 | 18,692 | 116,293 |
| Tropical storm profiles | 18,316 | 11,134 | 5,708 | 17,500 | 11,268 | 63,926 |
| Weak Hurricane profiles | 10,142 | 3,722 | 2,176 | 5,467 | 3,355 | 24,846 |
| Major Hurricane profiles | 1,782 | 2,013 | 659 | 1,879 | 835 | 7,168 |
| All TC profiles | 30,240 | 16,869 | 8,543 | 24,862 | 15,458 | 95,956 |

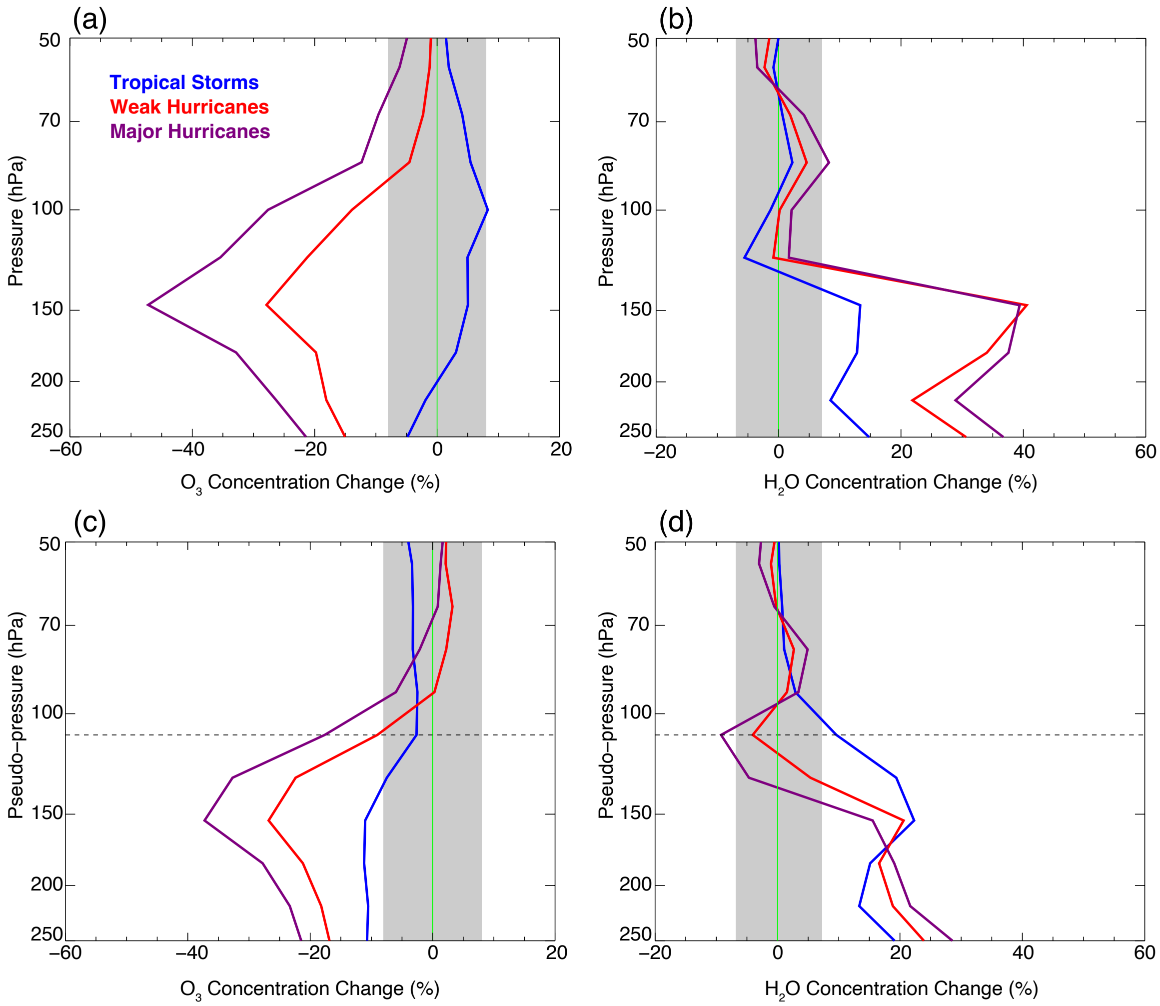


Figure 2.3: Composition change in TCs of tropical storm intensity (blue), hurricane intensity (red), and major hurricane intensity (purple) relative to non-TC profiles (light green reference lines). The dashed line represents the tropopause. Panels (a) and (b) show intensity dependency of ozone and water vapor respectively in raw pressure coordinates, while panels (c) and (d) show intensity dependency of ozone and water vapor in tropopause-relative coordinates. The gray color-filled bars in each panel represent the typical uncertainty of an individual MLS measurement. Analysis includes approximately 63,000 tropical storm profiles, 24,000 weak hurricane profiles, and 7,100 major hurricane profiles.

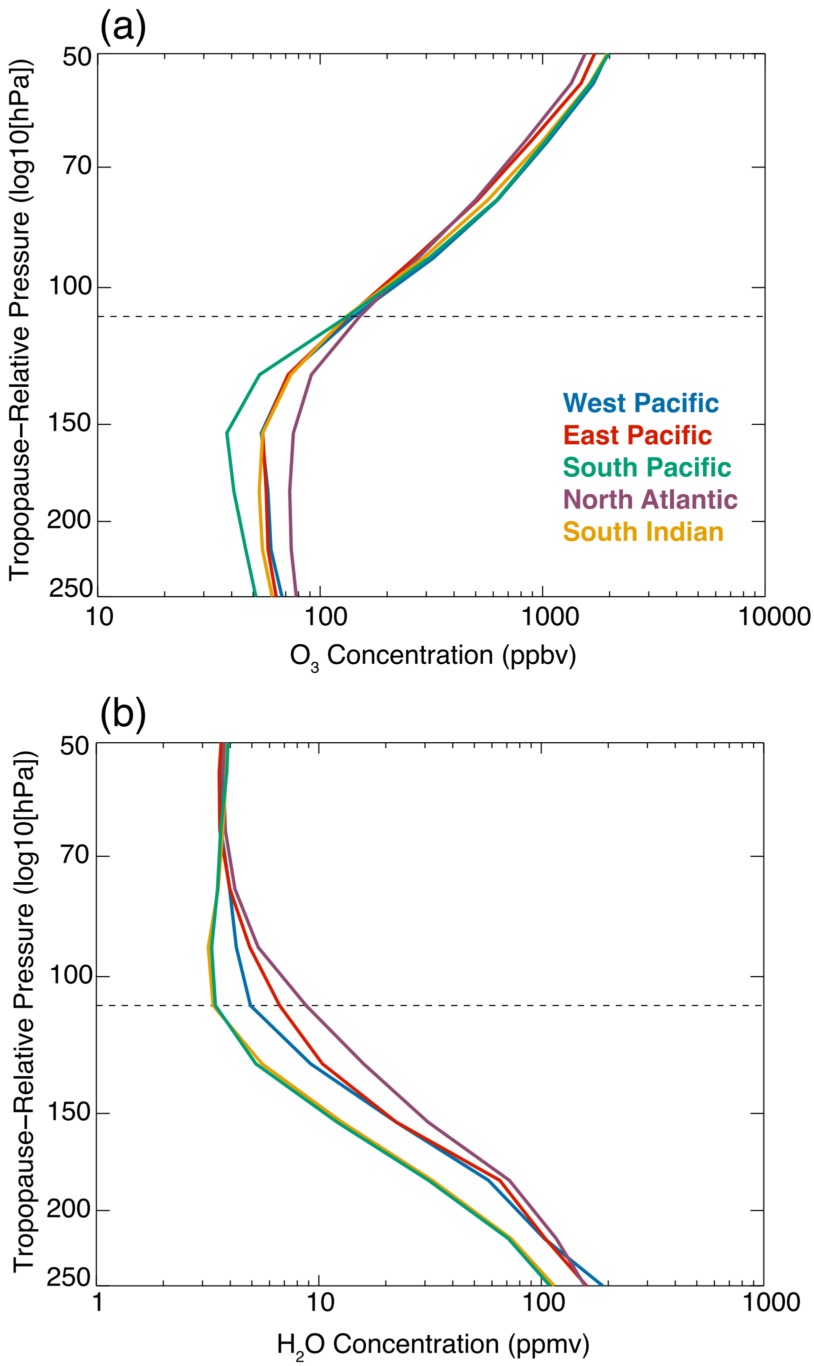


Figure 2.4: Background concentrations of UTLS ozone (a) and water vapor (b) in all analyzed basins plotted in tropopause relative coordinates. Colors corresponding to each basin are defined on the plot.

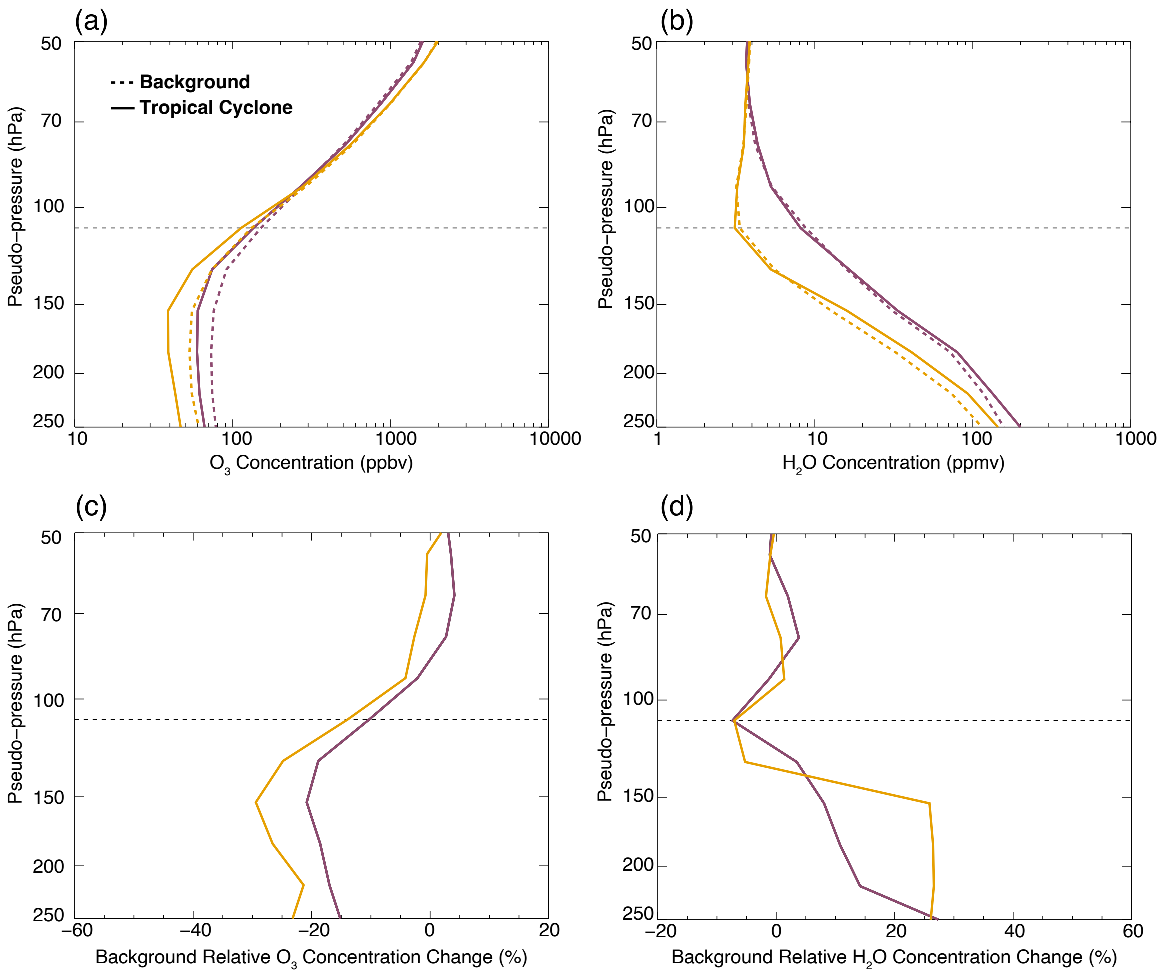


Figure 2.5: Panels (a) and (b) show the tropopause-relative absolute concentrations of ozone and water vapor, respectively, for the North Atlantic (purple) and South Indian (orange) ocean basins, with hurricane profiles represented by solid colored lines and background profiles represented by dashed colored lines. Plots c and d are as above, but with percent change relative to respective basin background conditions. The black dashed line represents the tropopause on each panel.

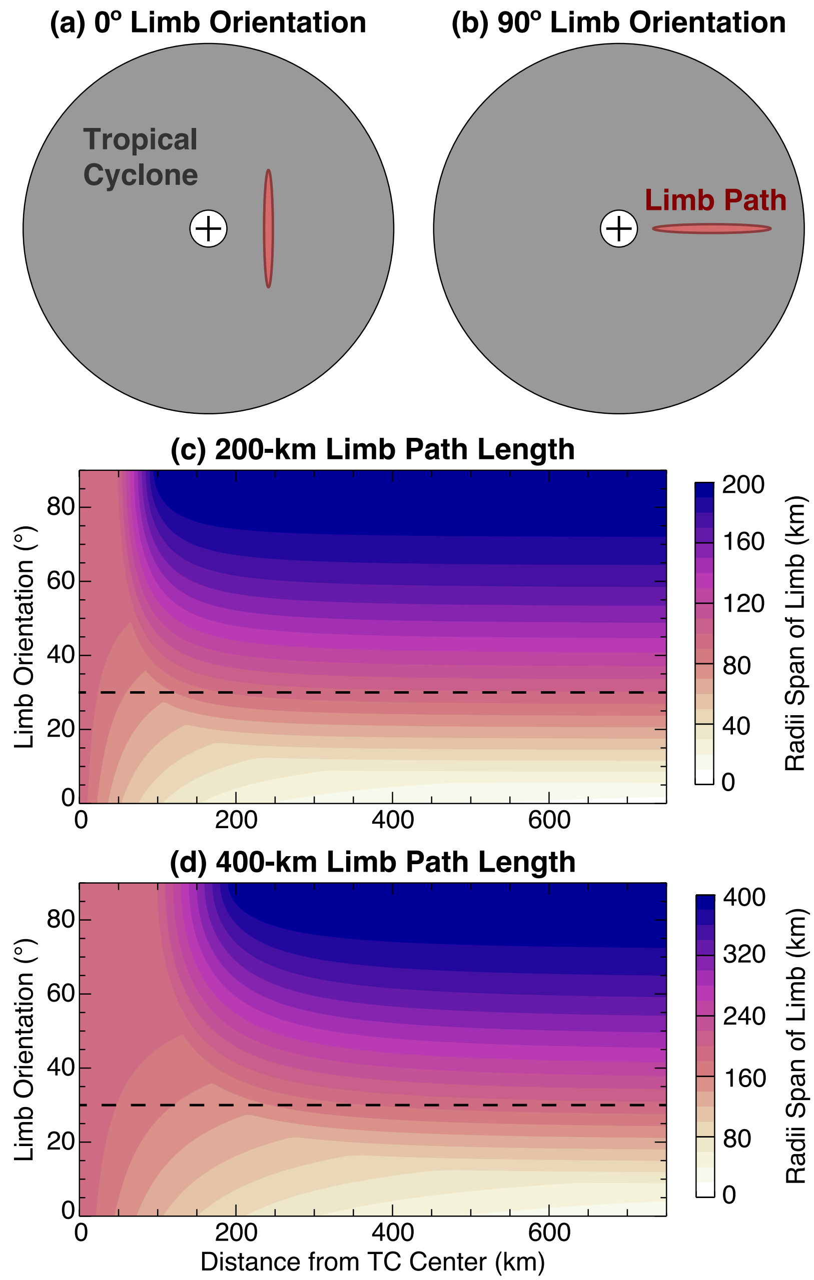


Figure 2.6: An illustration of the impact of MLS limb path geometry on the distances from TC center (radii) spanned by a measurement. Panels (a) and (b) show limb orientations of 0° (perpendicular to TC center) and 90° (parallel to TC center), respectively. Panels (c) and (d) show resulting radii spanned by a limb measurement as a function of distance from TC center and limb orientation for limb lengths of 200 km and 400 km, respectively. The dashed black lines in (c) and (d) lie at a limb orientation of 30°.

# Chapter 3

# Results

## 3.1 Intensity dependency

To examine the relationship between TC intensity and UTLS composition change, TC profiles can be grouped based on sustained wind speed. We create three intensity categories: tropical storm intensity (TC profiles with 10-m sustained wind speeds 35–63 kts), weak hurricane intensity (sustained wind speeds of 64–95 kts), and major hurricane intensity (sustained wind speeds $\geq$96 kts). Given the distance dependency of STE processes (see Section 3.2), we require all profiles used for intensity analysis to be within 300 km of TC center (approximately encompassing the inner core of the TC) and employ the limb geometry criteria as defined in Section 2.6. After profiles are filtered and sorted by intensity, average basin-relative composition changes are computed at tropopause-relative altitude.

UTLS $O_3$ changes are found to be highly sensitive to TC intensity. In Figure 3.3a, there is nearly an 80% average decrease in upper tropospheric $O_3$ concentration in major hurricanes; this decrease is only $\approx$40% in tropical storms. Additionally, the deficit is more pronounced within major hurricanes near the tropopause and into the lower stratosphere; the interquartile range plot in Figure 3.4a demonstrates a negative shift in the distribution of composition change for hurricane intensity storms, with the greatest decreases occurring for major hurricanes. This effect is diminished with altitude above the tropopause; apparent variations throughout most of the lower stratosphere are small enough to fall below the accuracy of individual MLS $O_3$ retrievals. Despite this, profiles demonstrate a clear relationship between TC intensity and UTLS $O_3$ concentration change, where stronger TCs are associated with a more prominent $O_3$ deficit in the UTLS, particularly near $\approx$2 km below the tropopause ($\sim$150 hPa). This result is consistent with the results of Zou and Wu (2005), who found that an increase in TC intensity was associated with decreased upper tropospheric $O_3$; however, our usage of higher sample sizes across multiple ocean basins provides additional evidence of the robustness of this relationship.

$H_2O$ within the UTLS (Fig. 3.3b) also shows high sensitivity to TC intensity, with stronger TCs resulting in larger increases in upper tropospheric $H_2O$ concentration, consistent with that found in Ray and Rosenlof (2007). The biggest differences in this study are found between tropical storms (average enhancements of up to 50% in the upper troposphere) and weak hurricanes (enhancements of nearly 80%). The differences between weak hurricanes and major hurricanes are comparably minor, with relatively overlapping distributions throughout the UTLS (see Fig. 3.4b) except for a significantly drier tropopause within major hurricanes, as found in Jiang et al. (2020) and expected due to previously-diagnosed tropopause cooling and lifting. In particular, the tropopause-level $H_2O$ concentration is around 20% lower than the typical background concentrations within major hurricanes; this feature is not present within tropical storms. Finally, a lower stratospheric hydration signal is strongest for major hurricanes, where $H_2O$ concentrations increase by more than 10% on average $\approx$2 km above tropopause ($\sim$80 hPa). This can be seen in the shifting of interquartile ranges for major hurricanes in particular (Fig 3.4b), where more subtle increases are found for weak hurricanes and tropical storms. Overall, there is a clear link between TC intensity and UTLS $H_2O$ change.

## 3.2 Distance dependency

To evaluate the relationship between UTLS composition change and distance from TC center we bin tropopause- and basin-relative profiles every 100 km and employ the limb geometry constraints from Section 2.6 for all bins except that closest to TC center. Due to higher resolution of MLS $H_2O$ retrievals, the innermost 100 km from TC center is divided further into 50-km bins. Additionally, only hurricanes are included in this analysis since UTLS impacts from tropical storms are comparatively weak. These constraints ensure an accurate accumulation of UTLS composition changes.

The resultant analysis for $O_3$ (Fig. 3.5a) demonstrates an intense and significant upper tropospheric deficit. The intensity of this deficit is maximized near TC center and decreases with distance, with the maximum change in $O_3$ concentration centered just below the tropopause. Additionally, this $O_3$ deficit weakly extends into the lower stratosphere, particularly within the inner 200 km of the storm, mirroring $O_3$ decreases near hurricanes found by Zou and Wu (2005). Although previous studies indicate that subsidence within the eye of the TC could enhance upper tropospheric $O_3$, this effect is not evident in this analysis. However, given that the 100-km bin size of $O_3$ observations is significantly larger than a typical TC eye and the MLS limb retrieval path for $O_3$ will span up to 200 km from TC center even when coincident, this is not surprising. Namely, previous work has indicated the subsidence feature is most evident within 50 km of TC center and is adjacent to the strongest vertical transport of $O_3$-poor air within deep convection of the eyewall (Gordon and Homeyer 2025). The competition between the narrow subsidence and broader eyewall convection likely obscures potential upper tropospheric $O_3$ increases from observation by MLS. Despite this, these results demonstrate a clear relationship between a change in UTLS $O_3$ concentration and distance from the center of a TC, as $O_3$ changes are most robust near TC center; therefore, distance from TC center is an important consideration when evaluating UTLS $O_3$ change.

UTLS $H_2O$ changes in TCs are also largely significant and dependent on distance from TC center. Figure 3.5b shows that TCs result in strong hydration of the upper troposphere, with average changes in $H_2O$ exceeding 50%. These effects decrease with distance, especially beyond 400 km from TC center. Additionally, weak hydration is observed in the lower stratosphere, particularly within the inner 200 km, where average $H_2O$ increases of 10–15% are present. Finally, there is a clear reduction in $H_2O$ at all distances from TC center evaluated that is coincident with the tropopause. This result is in agreement with Jiang et al. (2020), who found TC-induced adiabatic lift created a cold anomaly above the tropopause. This feature was found to enhance $H_2O$ deposition on TC-lofted cloud ice, which subsequently falls to lower altitudes, thereby drying the tropopause. We find that this feature is most prominent within 50–100 km from TC center and significant despite smaller sample sizes within this bin, although weak tropopause dehydration is observed ubiquitously beyond the center of the storm. Thus, we conclude that UTLS $H_2O$ impacts are highly dependent on distance, especially at altitudes removed from the tropopause.

## 3.3 Shear Dependency

To evaluate environmental influence on STE within TCs, we examine the effects of deep-layer vertical wind shear on UTLS composition change. For hurricanes only, we group MLS profiles by shear magnitude into 3 classes: weak shear ($< 5$ m s$^{-1}$), moderate shear (5–10 m s$^{-1}$), and strong shear ($> 10$ m s$^{-1}$). Given the demonstrated relationship between TC convection and deep-layer shear, we further classify profiles as located upshear or downshear of TC center and apply the limb geometry constraint. Finally, as also done for the TC intensity analysis, we include only profiles within 300 km from TC center.

Our results show a minor shear dependency for upper tropospheric $O_3$ and a substantial shear dependency for UTLS $H_2O$. When examining UTLS $O_3$, upper tropospheric deficits are stronger on the downshear side of the storm (Fig. 3.1a). These differences are most apparent in strongly sheared environments, where average upper tropospheric $O_3$ decreases upshear are around 50% compared to 70% downshear. However, closer to the tropopause and into the stratosphere, these differences become negligible. There are limited differences between weak, moderate, and strong shear profiles otherwise, apart from a tendency for a reduced depth of $O_3$ deficits with increasing shear (especially on the upshear side); there is significant overlap between the interquartile ranges of each shear category (see Fig. 3.2). In contrast, UTLS $H_2O$ shows substantial sensitivity to deep-layer shear (Fig. 3.1b). In the upper troposphere, upshear profiles have substantially higher $H_2O$ than downshear profiles when shear is weak (around a 60% average increase in $H_2O$ for downshear profiles, while upshear profiles have a nearly 100% average increase in upper tropospheric $H_2O$). In moderate shear environments, upshear and downshear profiles are nearly identical; however, in strong shear environments, upper tropospheric $H_2O$ is generally higher for downshear profiles closer to the tropopause. Given that the downshear side of the storm generally has the strongest convection in a sheared environment, while upshear locations have weaker updrafts (DeHart et al. 2014), these differences make sense. Notably, tropopause dehydration is the most prominent in low shear environments, where an average $H_2O$ decrease of $\sim$20% is observed; this dehydration feature is completely absent in strongly sheared environments. Finally, UTLS $H_2O$ shows much stronger sensitivity to shear magnitude on the upshear side of the storm than downshear; there is much more variability in the interquartile ranges of upshear profiles than downshear profiles within the UTLS (See Fig. 3.2) Thus, we find that upper tropospheric $O_3$ changes are somewhat dependent on deep-layer wind shear, while UTLS $H_2O$ changes are highly affected by shear.

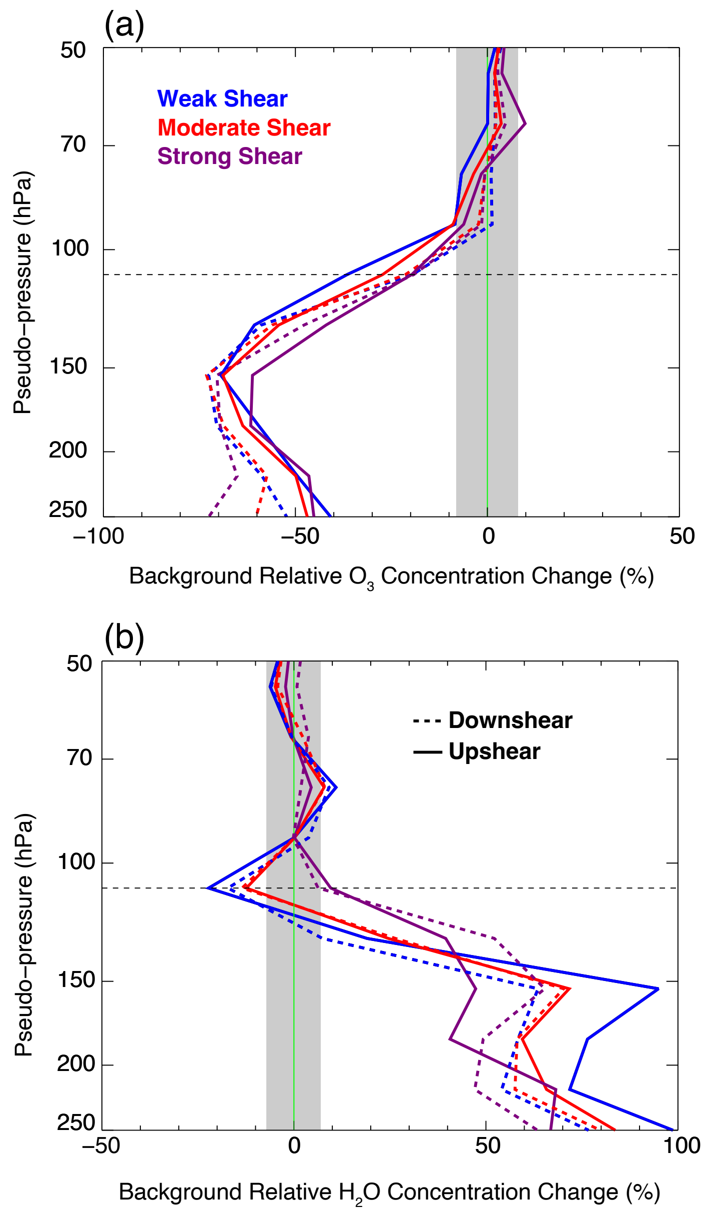


Figure 3.1: Basin and tropopause-relative plot showing the percent change of (a) UTLS ozone and (b) UTLS water vapor for hurricanes in environments with weak shear in blue, moderate shear in red, and strong shear in purple. The solid colored lines represent upshear profiles, while the dotted colored lines represent downshear profiles. The dotted black line represents the tropopause, the green line marks a 0% change, and the gray color-fill represents the typical uncertainty of an MLS measurement. Analysis includes approximately 150 hurricane profiles for weak shear cases, 500 profiles for moderate shear cases, and 130 profiles for strong shear cases for upshear and downshear analysis.

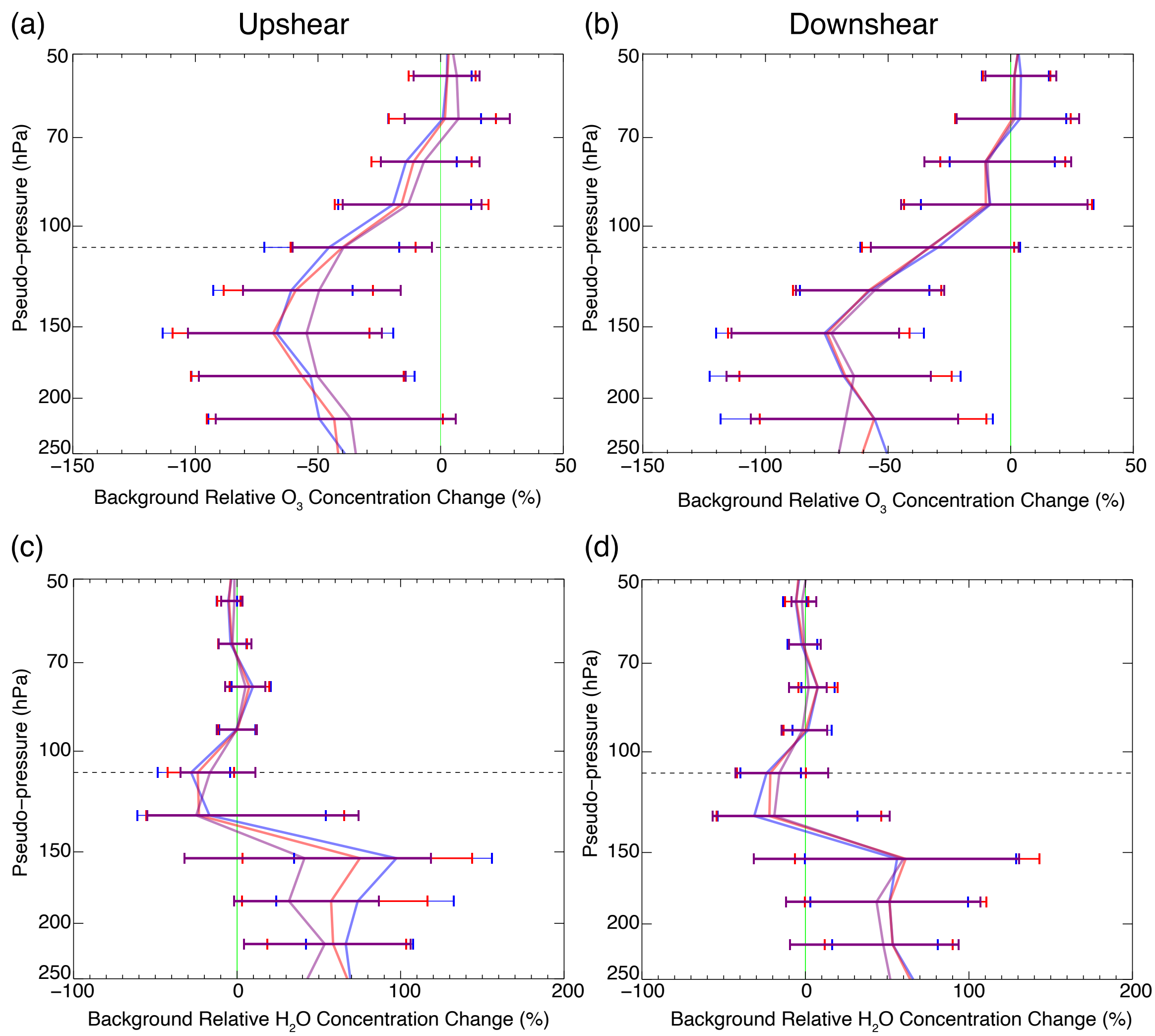


Figure 3.2: Basin and tropopause-relative plot showing the percent change of UTLS ozone (panels a and b) and UTLS water vapor (panels c and d) for hurricanes in environments with weak shear in blue, moderate shear in red, and strong shear in purple. Analysis is divided into upshear profiles (panels a and c) and downshear profiles (panels b and d). The solid colored lines represent median percent changes, while the bars represent the interquartile range for each shear intensity. The dotted black line represents the tropopause and the green line marks a 0% change. Analysis includes approximately 150 hurricane profiles for weak shear cases, 500 profiles for moderate shear cases, and 130 profiles for strong shear cases for upshear and downshear analysis.

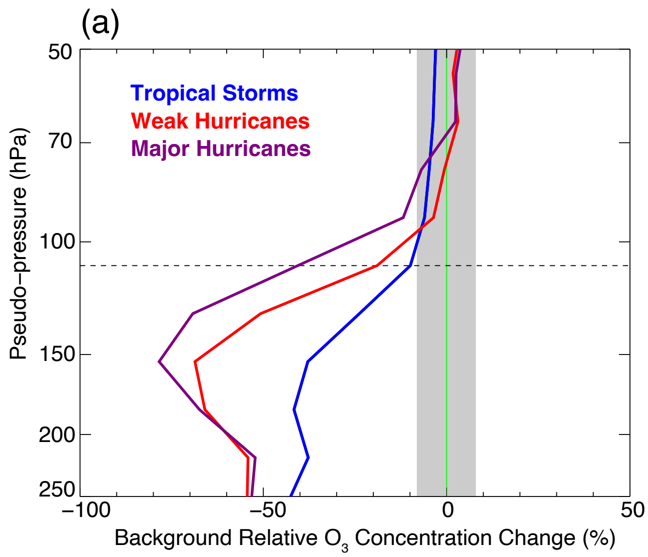


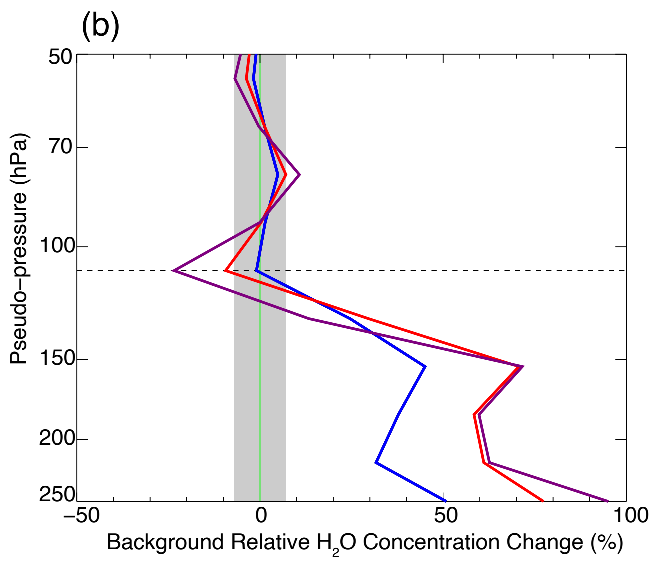


Figure 3.3: Basin-relative plot showing the percent change of (a) UTLS ozone and (b) UTLS water vapor partitioned by TC intensity and in tropopause relative coordinates. The purple line represents major hurricane intensity, the red line is weak hurricane intensity, and the blue line is tropical storm intensity. The horizontal black dashed line represents the tropopause, while the gray color-fill represents the typical uncertainty of an MLS measurement. A green line has been added at 0% concentration change (i.e., indicating the background). Analysis includes approximately 1900 TC profiles for tropical storms, 750 profiles for weak hurricanes, and 240 profiles for major hurricanes.

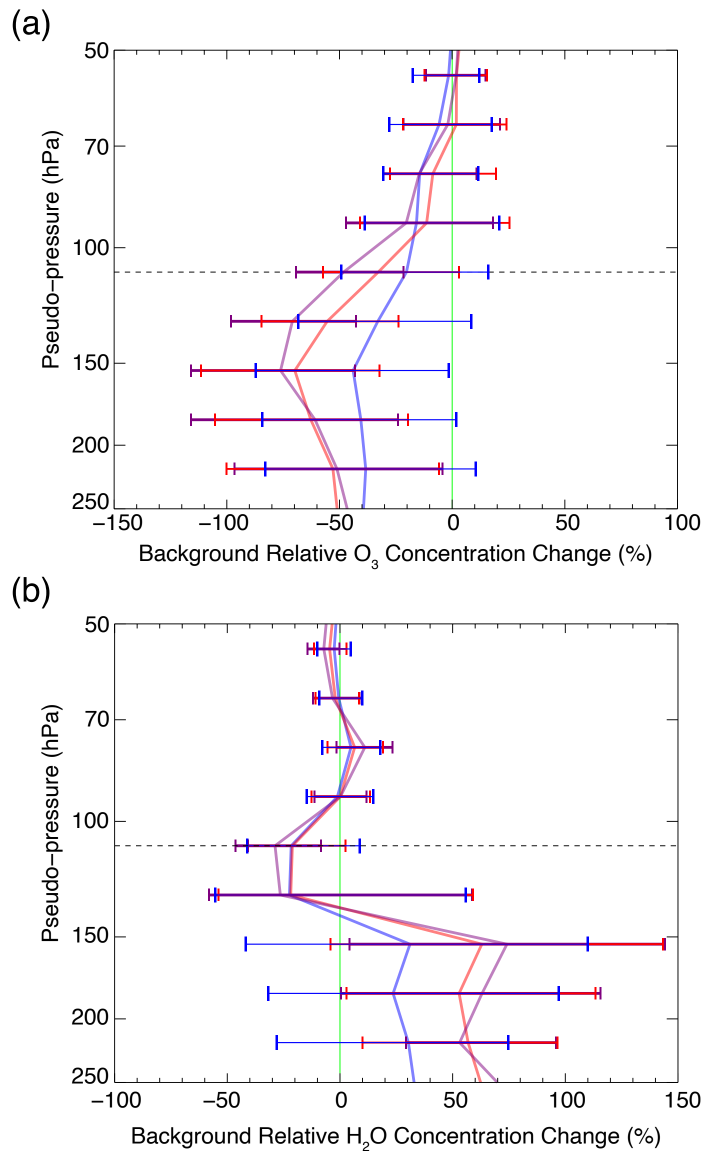


Figure 3.4: Basin-relative plot showing the percent change of (a) UTLS ozone and (b) UTLS water vapor partitioned by TC intensity and in tropopause relative coordinates. The purple line represents major hurricane intensity, the red line is weak hurricane intensity, and the blue line is tropical storm intensity. The solid colored lines represent median percent changes, while bars represent the interquartile range for each intensity category. A green line has been added at 0% concentration change (i.e., indicating the background). Analysis includes approximately 1900 TC profiles for tropical storms, 750 profiles for weak hurricanes, and 240 profiles for major hurricanes.

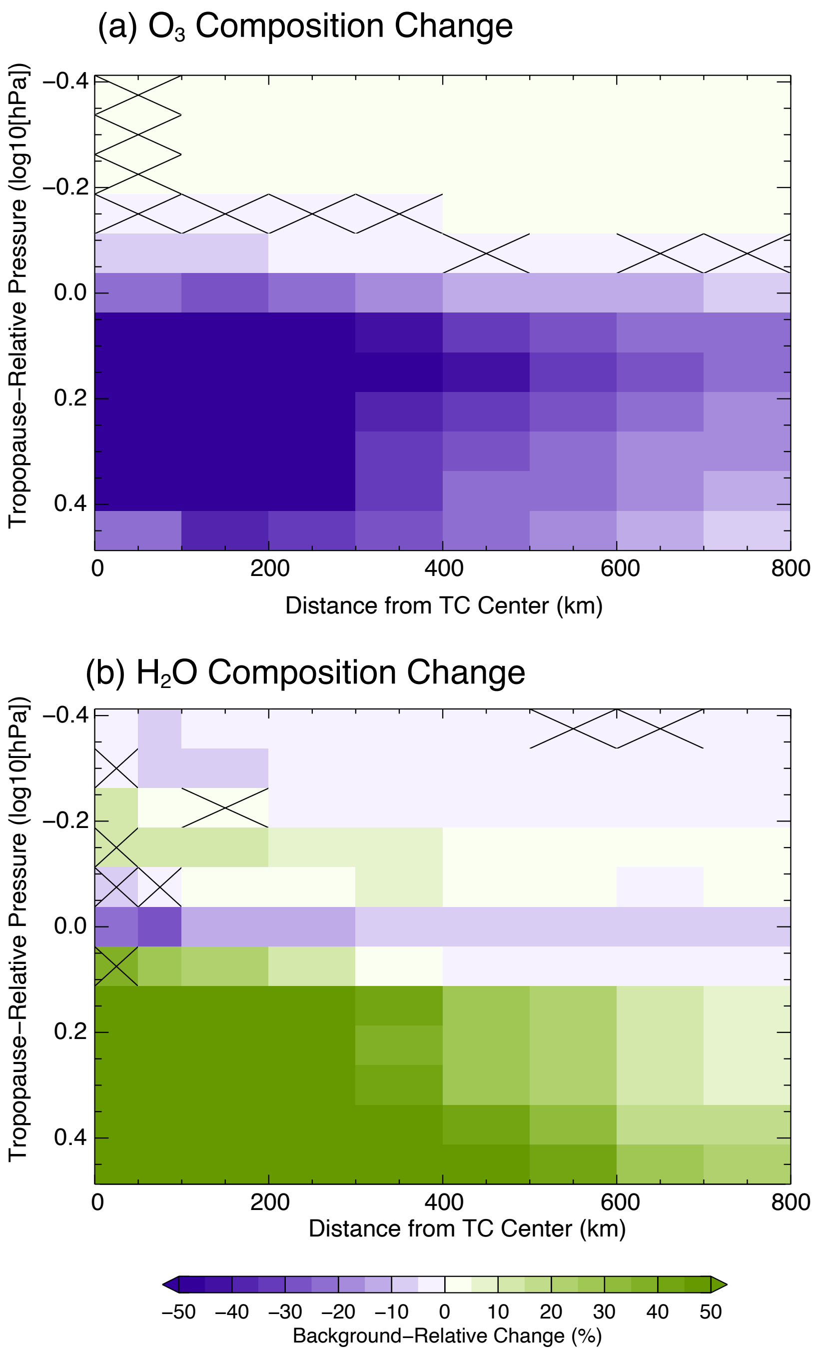


Figure 3.5: Basin-relative plot showing the percent change of (a) UTLS ozone and (b) UTLS water vapor as a function of distance from TC center and in relative pressure to the tropopause. An x is drawn over bins with a p-value greater than 0.01.

# Chapter 4

## Summary and Conclusions

This study leveraged 17 years of satellite observations to examine the influence of TCs on UTLS composition. In particular, we examined the environmental wind shear, distance and TC intensity dependency of TC-induced changes in UTLS $O_3$ and $H_2O$. To do this, we matched Aura MLS trace gas profiles with TC location data from the IBTrACS dataset and environmental conditions from MERRA-2 reanalysis. Given variation in tropopause height across profiles, we employed a tropopause-relative framework to allow for robust assessment of TC-induced composition change (see Fig. 2.3), a first for such studies. Additionally, we found that UTLS background $O_3$ and $H_2O$ concentrations vary significantly by ocean basin, sometimes by a factor of three times or more (see Figs. 2.4 & 2.5); therefore, TC-induced composition changes must also be calculated relative to the average background to be reliable when considering global samples.

Ultimately, we found that UTLS composition changes from TCs are dependent on both TC intensity and distance from TC center, while shear dependency was most evident for UTLS $H_2O$. We found that more intense TCs were associated with greater changes in UTLS composition (Fig. 3.3). In particular, we found that within major hurricanes, upper tropospheric $O_3$ decreased by nearly 80% on average. This strong upper tropospheric deficit is in agreement with the results of Zou and Wu (2005), who found decreased $O_3$ in hurricanes, especially in more intense storms. We uniquely demonstrate that this result is robust when assessed globally and for a much longer record, and further reveal the variation in $O_3$ composition impacts with altitude and for weaker TCs. For UTLS $H_2O$, we found strong upper tropospheric hydration of $\approx$70% on average within hurricanes, also in agreement with past work (e.g., Ray and Rosenlof 2007). We also robustly diagnosed hydration in the stratosphere, where increasing intensity is related to increasing hydration up to a maximum of ≈10% in major hurricanes at altitudes ≈2 km above tropopause (see Figs. 3.3 & 3.5), supporting similar results for select basins and limited samples in prior work (Ratnam et al. 2016; Jiang et al. 2020). Again, the detailed variation in altitude and robust global assessment in this study provide greater confidence in and assessment of these outcomes.

We also found that effects on UTLS $O_3$ and $H_2O$ generally decrease with distance from TC center, particularly beyond around 400 km (Fig. 3.5). In this analysis, the strongest stratospheric hydration signal was found to be within 100 km from TC center and at altitudes ≈1.5–3.5 km above tropopause, mirroring a similar result from a recent idealized modeling study (Gordon and Homeyer 2025). Additionally, we found a dehydrated tropopause within TCs, especially so within 50-100 km from TC center; this dehydrated tropopause agrees with findings from Jiang et al. (2020). The tropopause-level dehydration was found to be around 20% within major hurricanes (Fig. 3.3b) and only revealed when assessing composition change in tropopause-relative coordinates.

For UTLS composition change sensitivity to deep-layer wind shear, we found that upper tropospheric $O_3$ deficits are highest on the downshear side of TCs (Fig. 3.1a). Additionally, we found that UTLS $H_2O$ demonstrated a substantial sensitivity to shear, with weak shear environments having stronger UTLS composition changes (Fig. 3.1b). Upper tropospheric $H_2O$ change varied significantly between upshear and downshear profiles in both strong and weak shear environments, with limited differences when shear was moderate. A cautionary note to these shear sensitivities is that TC intensity is also affected by deep-layer wind shear (stronger shear typically weakens TCs), so the diagnosed sensitivities of UTLS composition change to TC intensity and deep-layer wind shear are not entirely independent.

Overall, it is clear from combination of prior studies and our work that STE within TCs significantly modifies $O_3$ and $H_2O$ composition throughout the UTLS, with impacts strongly affected by storm intensity and distance from TC center; a weaker TC or distances further away from a storm will generally have reduced UTLS composition impacts. The sensitivity of UTLS composition impacts to TC intensity warrants greater attention to the projected increase in TC intensity in the future as the climate warms (Emanuel 1987). Increased STE and UTLS $O_3$ and $H_2O$ change will amplify the radiative feedbacks driving climate warming, though which effect will dominate in TCs remains unknown. For example, decreased UTLS $O_3$ in TCs would reduce or slow warming, while increased UTLS $H_2O$ would enhance or accelerate warming. Thus, the prevailing climate impacts from STE in TCs are in competition and require further detailed study.

While our results provide robust insights into the impact of TCs on the UTLS, several limitations remain. Most notably, given the coarse resolution of MLS observations, this analysis does not allow for evaluation of distinct STE processes within TCs but rather the overall STE budget. Further, due to limb length restrictions, we cannot resolve distance-dependent composition change in bins smaller than 100 km for $O_3$ and 50 km for $H_2O$. Thus, although previous work has found subsidence within the eye of TCs (Rodgers et al. 1990; Leclair De Bellevue et al. 2006; Baray et al. 1999; Gordon and Homeyer 2025), it is not possible to diagnose the effect of this process using MLS observations; ultimately, we find significant upper tropospheric $O_3$ decreases within the inner 100 km of a TC (Fig. 3.3a), implying this region is dominated by lofted lower troposphere low-$O_3$ air. Additionally, given TC track data does not include information about the size and location of specific TC features (such as the eye, eyewall convection, inner core, rainbands, and extent of upper tropospheric outflow), we cannot relate observed composition change to such TC structure with confidence. Finally, although overall TC sample sizes are large in this study, sample sizes remain prohibitively limited for distant-dependent analysis of major hurricanes only, despite our results showing that major TCs have the largest impacts on UTLS composition within the inner core (Fig. 3.3). Even so, this analysis shows that both weak and major hurricanes have similar overall composition change patterns; therefore, our results using all hurricane samples are likely representative of the patterns seen within major hurricanes but biased toward relatively low amplitudes of composition change.

Given the relationship between UTLS composition change and Earth's radiation budget, as well as the disproportionate influence of TCs on STE (Zhan and Wang 2012), deepening our understanding of STE within TCs remains an important focus for future work. Specifically, further research is needed to determine the impact of individual transport processes such as stratospheric subsidence near TC center on UTLS composition change, given conflicting past work regarding the significance of such transport (e.g. Rodgers et al. 1990; Joiner et al. 2006), as well as overshooting. Additionally, analysis of a longer record of major hurricanes should be leveraged to further explore their impacts on UTLS composition. This is particularly relevant because although overall TC frequency is expected to decrease as the climate warms, the frequency of intense storms is expected to increase Knutson et al. (2010). Because our results show the most intense UTLS composition changes result from major hurricanes, examining the effects of projected TC frequency and intensity change on future UTLS composition modifications is of critical importance. Additionally, although we find that TCs significantly alter the UTLS, the persistence of these changes remains unclear and requires further investigation. Finally, this study does not consider UTLS changes resulting from TCs undergoing extratropical transition; further research is still needed to quantify these impacts. Despite this, our findings contribute to a growing body of evidence regarding the importance of evaluating TC-induced STE and its effects on UTLS composition.

## Bibliography


Allison, T., H. Fuelberg, and N. Heath, 2018: Simulations of vertical water vapor transport for tc ingrid (2013). *Journal of Geophysical Research: Atmospheres*, **123 (15)**, 8255–8282, https://doi.org/10.1029/2018JD028334.

Banerjee, A., G. Chiodo, M. Previdi, M. Ponater, A. J. Conley, and L. M. Polvani, 2019: Stratospheric water vapor: an important climate feedback. *Climate Dynamics*, **53 (3)**, 1697–1710, https://doi.org/10.1007/s00382-019-04721-4.

Baray, J.-L., G. Ancellet, T. Randriambelo, and S. Baldy, 1999: Tropical cyclone marlene and stratosphere-troposphere exchange. *Journal of Geophysical Research: Atmospheres*, **104 (D11)**, 13 953–13 970, https://doi.org/10.1029/1999JD900028.

Brewer, A. W., 1949: Evidence for a world circulation provided by the measurements of helium and water vapour distribution in the stratosphere. *Quarterly Journal of the Royal Meteorological Society*, **75 (326)**, 351–363, https://doi.org/10.1002/qj.49707532603.

Butchart, N., 2014: The brewer-dobson circulation. *Reviews of Geophysics*, **52 (2)**, 157–184, https://doi.org/10.1002/2013RG000448.

Chen, S. S., J. A. Knaff, and F. D. Marks, 2006: Effects of vertical wind shear and storm motion on tropical cyclone rainfall asymmetries deduced from TRMM. *Mon. Wea. Rev.*, **134**, 3190–3208.

Danielsen, E. F., 1993: In situ evidence of rapid, vertical, irreversible transport of lower tropospheric air into the lower tropical stratosphere by convective cloud turrets and by larger-scale upwelling in tropical cyclones. *Journal of Geophysical Research: Atmospheres*, **98 (D5)**, 8665–8681, https://doi.org/10.1029/92JD02954.

DeHart, J. C., R. A. Houze, and R. F. Rogers, 2014: Quadrant distribution of tropical cyclone inner-core kinematics in relation to environmental shear. *Journal of the Atmospheric Sciences*, **71 (7)**, 2713 – 2732, https://doi.org/10.1175/JAS-D-13-0298.1.

Dobson, G. M. B., 1956: Origin and distribution of the polyatomic molecules in the atmosphere. *Proceedings of the Royal Society of London. Series A. Mathematical and Physical Sciences*, **236 (1205)**, 187–193, https://doi.org/10.1098/rspa.1956.0127.

Emanuel, K., 1987: The dependence of hurricane intensity on climate. *Nature*, **326**, 483–485, https://doi.org/10.1038/nature03906.

Gelaro, R., and Coauthors, 2017: The modern-era retrospective analysis for research and applications, version 2 (merra-2). *Journal of Climate*, **30 (14)**, 5419 – 5454, https://doi.org/10.1175/JCLI-D-16-0758.1.

Gordon, A. E., and C. R. Homeyer, 2025: Examining stratosphere-troposphere exchange in tropical cyclones using idealized simulations. *J. Geophys. Res. Atmos.*, **conditionally accepted**.

Griffin, S. M., 2017: Climatology of tropical overshooting tops in north atlantic tropical cyclones. *Journal of Applied Meteorology and Climatology*, **56 (6)**, 1783 – 1796, https://doi.org/10.1175/JAMC-D-16-0413.1.

Hence, D. A., and R. A. Houze, 2011: Vertical structure of hurricane eyewalls as seen by the TRMM precipitation radar. *J. Atmos. Sci.*, **68**, 1637–1652, https://doi.org/10.1175/2011JAS3578.1.

Holton, J. R., P. H. Haynes, M. E. McIntyre, A. R. Douglass, and L. Pfister, 1995: Stratosphere-troposphere exchange. *Rev. Geophys.*, **33 (4)**, 403–439, https://doi.org/10.1029/95RG02097.

Homeyer, C. R., and K. P. Bowman, 2021: A 22-year evaluation of convection reaching the stratosphere over the united states. *Journal of Geophysical Research: Atmospheres*, **126 (13)**, e2021JD034 808, https://doi.org/10.1029/2021JD034808.

Jellis, D., K. P. Bowman, and A. D. Rapp, 2023: Lifetimes of overshooting convective events using high-frequency gridded radar composites. *Monthly Weather Review*, **151 (8)**, 1979 – 1992, https://doi.org/10.1175/MWR-D-23-0032.1.

Jiang, B., W. Lin, C. Hu, and Y. Wu, 2020: Tropical cyclones impact on tropopause and the lower stratosphere vapour based on satellite data. *Atmos. Sci. Let.*, **21 (e1006)**, https://doi.org/10.1002/asl.1006.

Joiner, J., A. Vasilkov, K. Yang, and P. K. Bhartia, 2006: Observations over hurricanes from the ozone monitoring instrument. *Geophys. Res. Lett.*, **33 (L06807)**, https://doi.org/10.1029/2005GL025592.

Kaplan, J., and M. DeMaria, 2003: Large-scale characteristics of rapidly intensifying tropical cyclones in the north atlantic basin. *Wea. Forecasting*, **18**, 1093–1108.

Keyser, D., and M. A. Shapiro, 1986: A review of the structure and dynamics of upper-level frontal zones. *Monthly Weather Review*, **114 (2)**, 452 – 499, https://doi.org/10.1175/1520-0493(1986)114⟨0452:AROTSA⟩2.0.CO;2.

Kiehl, J. T., and K. E. Trenberth, 1997: Earth's annual global mean energy budget. *Bulletin of the American Meteorological Society*, **78 (2)**, 197 – 208, https://doi.org/10.1175/1520-0477(1997)078⟨0197:EAGMEB⟩2.0.CO;2.

Knapp, K. R., M. C. Kruk, D. H. Levinson, H. J. Diamond, and C. J. Neumann, 2010: The international best track archive for climate stewardship (IBTrACS). *Bull. Amer. Meteorol. Soc.*, **91**, 363–376, https://doi.org/10.1175/2009BAMS2755.1.

Knutson, T. R., and Coauthors, 2010: Tropical cyclones and climate change. *Nature Geoscience*, **3 (3)**, 157–163, https://doi.org/10.1038/ngeo779, URL https://doi.org/10.1038/ngeo779.

Lacis, A. A., D. J. Wuebbles, and J. A. Logan, 1990: Radiative forcing of climate by changes in the vertical distribution of ozone. *Journal of Geophysical Research*, **95**, 9971–9981, https://doi.org/10.1029/JD095iD07p09971.

Leclair De Bellevue, J., J. Baray, S. Baldy, G. Ancellet, R. Diab, and F. Ravetta, 2007: Simulations of stratospheric to tropospheric transport during the tropical cyclone marlene event. *Atmospheric Environment*, **41 (31)**, 6510–6526, https://doi.org/10.1016/j.atmosenv.2007.04.040.

Leclair De Bellevue, J., A. Réchou, J. L. Baray, G. Ancellet, and R. D. Diab, 2006: Signatures of stratosphere to troposphere transport near deep convective events in the southern subtropics. *Journal of Geophysical Research: Atmospheres*, **111 (D24)**, https://doi.org/10.1029/2005JD006947.

Liu, C., and E. A. Barnes, 2018: Quantifying isentropic mixing linked to rossby wave breaking in a modified lagrangian coordinate. *Journal of the Atmospheric Sciences*, **75 (3)**, 927 – 942, https://doi.org/10.1175/JAS-D-17-0204.1.

Livesey, N. J., and Coauthors, 2022: Earth Observing System (EOS) Aura Microwave Limb Sounder (MLS): Version 5.0x Level 2 and 3 data quality and description document. Tech. Rep. JPL D-105336 Rev. B, Jet Propulsion Laboratory, Available electronically from https://mls.jpl.nasa.gov/data/v5-0_data_quality_document.pdf.

McIntyre, M. E., and T. N. Palmer, 1983: Breaking planetary waves in the stratosphere. *Nature*, **305 (5935)**, 593–600, https://doi.org/10.1038/305593a0.

Merrill, R. T., 1988: Characteristics of the upper-tropospheric environmental flow around hurricanes. *Journal of Atmospheric Sciences*, **45 (11)**, 1665 – 1677, https://doi.org/10.1175/1520-0469(1988)045⟨1665:COTUTE⟩2.0.CO;2.

Millán, L., and Coauthors, 2022: The hunga tonga-hunga ha'apai hydration of the stratosphere. *Geophysical Research Letters*, **49 (13)**, e2022GL099 381, https://doi.org/10.1029/2022GL099381.

Newell, R. E., and Coauthors, 1996: Atmospheric sampling of supertyphoon mireille with nasa dc-8 aircraft on september 27,1991, during pem-west a. *Journal of Geophysical Research: Atmospheres*, **101 (D1)**, 1853–1871, https://doi.org/10.1029/95JD01374, https://agupubs.onlinelibrary.wiley.com/doi/pdf/10.1029/95JD01374.

Pan, L. L., S. B. Honomichl, T. V. Bui, T. Thornberry, A. Rollins, E. Hintsa, and E. J. Jensen, 2018: Lapse rate or cold point: The tropical tropopause identified by in situ trace gas measurements. *Geophysical Research Letters*, **45 (19)**, 10,756–10,763, https://doi.org/10.1029/2018GL079573.

Pommereau, J.-P., 2010: Troposphere-to-stratosphere transport in the tropics. *Comptes Rendus. Géoscience*, **342 (4-5)**, 331–338, https://doi.org/10.1016/j.crte.2009.10.015.

Preston, A. D., H. E. Fuelberg, and M. C. Barth, 2019: Simulation of chemical transport by typhoon mireille (1991). *Journal of Geophysical Research: Atmospheres*, **124 (21)**, 11 614–11 639, https://doi.org/10.1029/2019JD030446.

Ratnam, M. V., S. R. Babu, S. S. Das, G. Basha, B. V. Krishnamurthy, and B. Venkateswararao, 2016: Effect of tropical cyclones on the stratosphere–troposphere exchange observed using satellite observations over the north indian ocean. *Atmos. Chem. Phys.*, **16**, 8581–8591, https://doi.org/10.5194/acp-16-8581-2016.

Ray, E. A., and K. H. Rosenlof, 2007: Hydration of the upper troposphere by tropical cyclones. *J. Geophys. Res.*, **112 (D12311)**, https://doi.org/10.1029/2006JD008009.

Riese, M., F. Ploeger, A. Rap, B. Vogel, P. Konopka, M. Dameris, and P. Forster, 2012: Impact of uncertainties in atmospheric mixing on simulated utls composition and related radiative effects. *Journal of Geophysical Research: Atmospheres*, **117 (D16)**, https://doi.org/10.1029/2012JD017751.

Rodgers, E. B., J. Stout, J. Steranka, and S. Chang, 1990: Tropical cyclone-upper atmospheric interaction as inferred from satellite total ozone observations. *J. Appl. Meteor.*, **29**, 934–954.

Romps, D. M., and Z. Kuang, 2009: Overshooting convection in tropical cyclones. *Geophysical Research Letters*, **36 (9)**, https://doi.org/10.1029/2009GL037396.

Shapiro, M. A., 1980: Turbulent mixing within tropopause folds as a mechanism for the exchange of chemical constituents between the stratosphere and troposphere. *Journal of Atmospheric Sciences*, **37 (5)**, 994 – 1004, https://doi.org/10.1175/1520-0469(1980)037⟨0994:TMWTFA⟩2.0.CO;2.

Solomon, S., K. H. Rosenlof, R. W. Portmann, J. S. Daniel, S. M. Davis, T. J. Sanford, and G.-K. Plattner, 2010: Contributions of stratospheric water vapor to decadal changes in the rate of global warming. *Science*, **327 (5970)**, 1219–1223, https://doi.org/10.1126/science.1182488.

Tinney, E. N., and C. R. Homeyer, 2021: A 13-year trajectory-based analysis of convection-driven changes in upper troposphere lower stratosphere composition over the united states. *Journal of Geophysical Research: Atmospheres*, **126 (3)**, e2020JD033 657, https://doi.org/10.1029/2020JD033657.

World Meteorological Organization, 1957: Meteorology—a three-dimensional science: Second session of the commission for aerology. *World Meteorol. Organ. Bull.*, **4**, 134–138.

Wu, L., H. Su, X. Zeng, D. J. Posselt, S. Wong, S. Chen, and A. Stoffelen, 2024: Uncertainty of atmospheric winds in three widely used global reanalysis datasets. *J. Appl. Meteor. Climatol.*, **63**, 165–180, https://doi.org/10.1175/JAMC-D-22-0198.1.

Xian, T., and C. R. Homeyer, 2019: Global tropopause altitudes in radiosondes and reanalyses. *Atmos. Chem. Phys.*, **19**, 5661–5678, https://doi.org/10.5194/acp-19-5661-2019.

Zhan, R., and Y. Wang, 2012: Contribution of tropical cyclones to stratosphere-troposphere exchange over the northwest pacific: Estimation based on airs satellite retrievals and era-interim data. *J. Geophys. Res.*, **117 (D12112)**, https://doi.org/10.1029/2012JD017494.

Zou, X., and Y. Wu, 2005: On the relationship between total ozone mapping spectrometer (toms) ozone and hurricanes. *J. Geophys. Res.*, **110 (D06109)**, https://doi.org/10.1029/2004JD005019.